

1 **Diurnal cycle of iodine, bromine and mercury concentrations in Svalbard surface snow**

2 ¹Andrea Spolaor, ¹Elena Barbaro, ²David Cappelletti, ¹Clara Turetta, ³Mauro Mazzola, ⁴Fabio
3 Giardi, ⁵Mats P. Björkman, ⁶Federico Lucchetta, ¹Federico Dallo, ⁷Katrine Aspmo Pfaffhuber,
4 ⁸Hélène Angot, ⁹Aurelien Dommergue, ¹⁰Marion Maturilli, ¹¹Alfonso Saiz-Lopez, ^{6,1}Carlo Barbante
5 and ¹Warren RL Cairns

6
7 *¹Institute of Polar Sciences, ISP-CNR, Campus Scientifico Via Torino 155, 30172 Mestre, Venice,*
8 *Italy.*

9 *²Dipartimento di Chimica, Biologia e Biotecnologie, Università degli Studi di Perugia I-06123*
10 *Perugia, Italy*

11 *³National Research Council, Institute of Atmospheric Sciences and Climate, CNR-ISAC, Via P.*
12 *Gobetti 101, Bologna, Italy*

13 *⁴Chemistry Department – Analytical Chemistry, Scientific Pole, University of Florence, Via della*
14 *Lastruccia 3, I-50019 Sesto Fiorentino (Florence) Italy.*

15 *⁵University of Gothenburg, Department of Earth Sciences, Box 460, 40530 Göteborg, Sweden*

16 *⁶Ca' Foscari University of Venice, Department of Environmental Sciences, Informatics and*
17 *Statistics, Santa Marta – Dorsoduro 2137, 30123 Venice, Italy.*

18 *⁷NILU - Norwegian Institute for Air Research, Kjeller, Norway*

19 *⁸Institute of Arctic and Alpine Research (INSTAAR), University of Colorado, Boulder, USA*

20 *⁹Institut des Géosciences de l'Environnement, Univ. Grenoble Alpes, CNRS, IRD, Grenoble INP,*
21 *38000 Grenoble, France.*

22 *¹⁰Alfred Wegener Institute, Helmholtz Centre for Polar and Marine Research, Potsdam, Germany*

23 *¹¹Department of Atmospheric Chemistry and Climate, Institute of Physical Chemistry Rocasolano,*
24 *CSIC, Madrid, Spain*

25

26

27

28

29

30

31

32

33

34

35

36

37 **Abstract**

38 Sunlit snow is highly photochemically active and plays a key role in the exchange of gas-phase
39 species between the cryosphere to the atmosphere. Here, we investigate the behaviour of two
40 selected species in surface snow: mercury (Hg) and iodine (I). Hg can deposit year-round and
41 accumulate in the snowpack. However, photo-induced re-emission of gas-phase Hg from the
42 surface has been widely reported. Iodine is active in atmospheric new particle formation, especially
43 in the marine boundary layer, and in the destruction of atmospheric ozone. It can also undergo
44 photochemical re-emission. Although previous studies indicate possible post-depositional processes,
45 little is known about the diurnal behaviour of these two species and their interaction in surface snow.
46 The mechanisms are still poorly constrained, and no field experiments have been performed in
47 different seasons to investigate the magnitude of re-emission processes. Three sampling campaigns
48 conducted at an hourly resolution for 3-days each were carried out near Ny-Ålesund (Svalbard) to
49 study the behaviour of mercury and iodine in surface snow under different sunlight and
50 environmental conditions (24h-darkness, 24h-sunlight and day/night cycles). Our results indicate a
51 different behaviour of mercury and iodine in surface snow during the different campaign. The
52 day/night experiments demonstrate the existence of a diurnal cycle in surface snow for Hg and
53 iodine, indicating that these species are indeed influenced by the daily solar radiation cycle.
54 Differently bromine did not show any diurnal cycle. The diurnal cycle also disappeared for Hg and
55 iodine during the 24h-sunlight period and during 24h-darkness experiments supporting the idea of
56 the occurrence (absence) of a continuous recycling/exchange at the snow-air interface. These results
57 demonstrate that this surface snow recycling is seasonally dependent, through sunlight. They also
58 highlight the non-negligible role that snowpack emissions have on ambient air concentrations and
59 potentially on iodine-induced atmospheric nucleation processes.

60
61
62
63
64
65
66
67
68
69
70
71
72

73 **1. Introduction**

74 Polar Regions are being increasingly studied for their important roles in global climate and
75 atmospheric chemical cycles. Multiple studies have improved our understanding of atmospheric
76 processes in polar regions, ranging from new particle formation processes (Dall'Osto et al., 2017;
77 Sipilä et al., 2016), ozone destruction processes (Saiz-Lopez et al., 2007; Simpson et al., 2007), the
78 role of halogens in polar atmospheric processes (Saiz-Lopez and von Glasow, 2012; Spolaor et al.,
79 2013a), the mercury cycle (Angot et al., 2016a; Aspino et al., 2005; **Brooks et al., 2006**;
80 Dommergue et al., 2003a; Durnford and Dastoor, 2011; **Skov et al., 2006**) to atmospheric transport
81 and deposition of natural and anthropogenic compounds (Moroni et al., 2015; Moroni et al., 2017;
82 Udisti et al., 2016; Zangrando et al., 2013). The Polar Regions are characterized by periods with 24
83 h of continuous solar radiation (April to September in the Arctic), periods when the night and day
84 cycle is present (February to March and September to October in the Arctic) and periods of
85 continuous darkness (November to January in the Arctic), the so-called polar night. The different
86 periods have completely different environmental conditions depending on the incoming solar
87 radiation, with variables such as sea ice presence or biological activity being radically altered by
88 sunlight. One important aspect is snow cover. Annual snow is present, on average, for almost nine
89 months of the year and represents an important environmental component of Polar Regions. In
90 Svalbard, the snow starts to accumulate in October and remains until the end of May when the
91 melting season begins (Førland et al., 2011). However, with Arctic temperatures rising (Maturilli et
92 al., 2013), the length of the snow cover has diminished (Brage B. Hansen et al., 2014), with direct
93 consequences on the environment of the Svalbard archipelago, such as glacier mass loss, permafrost
94 thawing, disturbances of the local fauna etc. (Karner et al., 2013; Kohler and Aanes, 2004; Kohler
95 et al., 2007; Westermann et al., 2011). The annual snow layer is an extremely dynamic portion of
96 the cryosphere, and can be defined as the snow accumulated and present on the ground during the
97 whole year (Spolaor et al., 2016a). The characteristics of the annual snow strata are strongly
98 dependent on climate conditions and may influence food access for animals that rely on food
99 sources below the snow (Kohler and Aanes, 2004). From a chemical point of view, snow is a sink
100 for an impressive number of chemical compounds (natural and anthropogenic) and elements
101 (Björkman et al., 2013; Gabrieli et al., 2011; Vecchiato et al., 2018). Specific compounds and
102 elements accumulate during the winter can undergo photo-activation and can be re-emitted into the
103 atmosphere (Angot et al., 2016c; Spolaor et al., 2014), while taking part in numerous geochemical
104 and biological cycles (Björkman et al., 2014) during spring and summer. Mercury (Hg) and iodine
105 (I) are two elements that can be photo activated and released from the snow pack. Mercury is a
106 heavy metal with a known toxicity present in the environment in several different chemical forms.
107 It is reactive in the environment and undergoes photochemical reactions that change its speciation
108 and chemical behaviour (Dommergue et al., 2010; Durnford and Dastoor, 2011; Saiz-Lopez et al.,

109 2018; Steffen et al., 2002). Mercury in its oxidized form can be deposited onto the snowpack,
110 increasing Hg concentrations in the upper snow strata (Obrist et al., 2017). Once present in the
111 snowpack, Hg is very labile, and it can be reduced back to elemental Hg (Hg(0)) and undergo
112 dynamic exchange with the atmosphere (Song et al., 2018; Spolaor et al., 2018; Steffen et al., 2002).
113 The role of the snowpack is crucial in the mercury cycle in Polar Regions since it acts as both a sink
114 (deposition, accumulation) and a source (re-emission). Several studies have already been carried out
115 in the polar regions with the aim of determining the extent of mercury recycling between the
116 surface snow and the lower atmosphere (Angot et al., 2016c; Brooks et al., 2008; Brooks et al.,
117 2006; Dommergue et al., 2012; Douglas et al., 2008; Han et al., 2014; Obrist et al., 2017; Wang et
118 al., 2016). It has been shown that surface Arctic snow could lose up to 90 % of its total Hg content
119 within 48 hours (Poulain et al., 2004). Similar, re-emission/loss rates of Hg from snow surface (35–
120 50 %) and drifting snow (65–75 %) over 10.5 h have been suggested in chamber experiments
121 (Sherman et al., 2010) while, in a study performed on the Antarctic Plateau, Spolaor et al. 2018
122 suggest a loss of 90% of mercury in the upper snow layer within a few hours. High gaseous
123 elemental mercury (GEM) emission from the snow pack has also been determined at Station North
124 (Greenland) where the emission flux can rise up to $190 \text{ ng m}^{-2} \text{ min}^{-1}$ (Kamp et al., 2018). Similar to
125 mercury, iodine can undergo photochemical activation in surface snow resulting in its presence in
126 the surrounding atmosphere (Frieb et al., 2010; Spolaor et al., 2014). Several studies aimed at
127 understanding the behaviour of iodine in the Arctic region, from a paleo perspective using ice core
128 archives (Cuevas et al., 2018; Spolaor et al., 2016b), and field (atmospheric and snow) experiments
129 (Frieb et al., 2010; Gilfedder et al., 2007). The role of iodine in new particle formation as well in
130 ozone destruction is currently under investigation (Allan et al., 2015; Saiz-Lopez et al., 2012; Saiz-
131 Lopez, 2006; Sipilä et al., 2016) since it could have a direct effect on the radiative budget of polar
132 areas. Up to now, it was believed that iodine was mainly associated with biological emissions,
133 however, recent studies have underlined the increase in ocean inorganic emissions (tripled since
134 1950) connected with the increase in anthropogenic ozone via reactions over the ocean surface
135 (Cuevas et al., 2018). Like mercury, iodine could be released from surface snow and directly
136 participate in specific processes within the marine boundary layer, particularly in new particle
137 formation. Little information exists on the behaviour of mercury and iodine in surface snow during
138 different seasons. Laboratory experiments have been carried out to understand light-induced
139 processes regarding Hg and iodine (Durnford and Dastoor, 2011; Saiz-Lopez et al., 2012; Spolaor et
140 al., 2013b). However few experiments have been carried out in the field, with the specific aim of
141 understanding the diurnal dynamics of these elements in surface snow (Dommergue et al., 2003b;
142 Ferrari et al., 2005; Spolaor et al., 2018)._The unique high-temporal resolution experiments
143 presented, aim to improve our understanding of the behaviour of these elements in the upper snow
144 layers (0-3 cm) under different light and atmospheric conditions to investigate their short-term

145 (diurnal) variation.

146

147 **2. Methods**

148 The experiments were conducted in the vicinity of Ny-Ålesund, in the snowfield behind the
149 Gruvebadet aerosol site (Figure 1). This area has a homogeneously flat surface without specific
150 elevation changes or obstacles that might interfere with snow deposition or wind-blown
151 redistribution. This area is approximatively 1 km from the coast line of the Kongsfjorden and about
152 400 m from the Zeppelin mountain. The “Gruvebadet” snow field is located to the south of Ny-
153 Alesund at an elevation of the 80 m a.s.l. (Figure 1). The “Gruvebadet” snow field is located to the
154 south of Ny-Ålesund, while the prevailing wind are mainly from east and south-east, minimizing
155 possible influences from station activities.

156

157

158 **2.1 Sampling period and strategy**

159 Surface snow samples were collected in the vicinity of Ny-Ålesund, specifically in the snow field
160 behind the “Gruvebadet” Aerosol Laboratory (Figure 1). Three experiments were conducted, two in
161 spring (2015 and 2016) and one in winter (2017). In 2015, we performed the first surface
162 experiment (hereafter called the “2015 experiment”) between the 28th of April and the 1st of May.
163 This period was characterized by 24 hours of sunlight (incoming solar radiation ranged from a
164 minimum of 25 Wm⁻² to a maximum of 456 W/m²). In 2016, a second experiment (hereafter called
165 the “2016 experiment”) was carried out between the 6th and the 9th of April when the night and day
166 cycle was still present at Ny-Ålesund (incoming solar radiation between 0 and 227 Wm⁻²). The last
167 experiment was conducted during the polar night, between the 24th and the 29th of January 2017
168 (hereafter called the “2017 experiment”) with the complete absence of incoming solar radiation.

169 *The 2017 experiment was conducted during the second half of January when full snow cover is*
170 *guaranteed (López-Moreno et al., 2016). In December, snow cover in the Spitsbergen area is not*
171 *homogeneously distributed. The ground could still be partially exposed, meaning that locally*
172 *generated windblown dust could affect the trace element concentrations in the snow surface. The*
173 *spring period selected for the 2016 experiment had two main characteristics: a well-defined night*
174 *and day cycle without a long sunset, avoiding possible incoming solar radiation by diffraction*
175 *processes over the horizon. There was also the possibility to observe atmospheric mercury depletion*
176 *events (AMDE) connected with bromine explosion events (Lu et al., 2001; Moore et al., 2014;*
177 *Schroeder and Munthe, 1998). Unfortunately, these events were not observed as the northern coast*
178 *of Svalbard was virtually ice free by the time we started sampling. The 2015 experiment was*
179 *scheduled to end at the beginning of May, when we have a full 24 h of sunlight reaching the snow*
180 *surface, but temperatures are still below freezing, avoiding/minimizing the confounding effects of*

181 snow pack melt or collapse on surface photochemical processes and gaseous mercury transport in
182 the interstitial air. The meteorological conditions throughout all the experiments are within the
183 expected local conditions for the time of year.

184 To determine the diurnal variation, and the rates of the expected changes in iodine and mercury
185 concentrations, a high temporal resolution (hourly) sampling strategy was adopted. An area of
186 approximately 2 m x 2 m was delimited for surface snow sampling, and all samples were collected
187 inside this delimited area. At the beginning of the experiment, six samples were collected to
188 evaluate the spatial variability of mercury, iodine, bromine (bromine is limited to the “2016
189 experiment”) and sodium in surface snow within the delimited snowfield. Afterwards, surface snow
190 (the first 3 cm) was sampled with an hourly resolution for three consecutive days. The upper 3 cm
191 were chosen as this is the snow layer that is most influenced by the surrounding atmospheric
192 conditions, and, in case of snowfall, by deposition (Spolaor et. al. 2018). This choice also
193 minimizes the effect of different physical snow conditions (density and crystal shape and size).
194 Although re-emission of mercury and iodine from lower snow strata could influence the gaseous
195 concentrations in the snow interstitial air (Fain et al., 2007) it is much less likely to have a direct
196 effect on snow concentrations due to its poor solubility in water. During snow sampling, the
197 temperature of surface snow was also measured. To minimize spatial variability, samples were
198 collected following a straight line leaving about 5 cm between each of the sampling points. After
199 collection, the snow samples were stored at -20°C in dark conditions and transported to the Venice
200 ISP-CNR laboratories. The samples were never melted or exposed to direct sunlight until analysis.

201

202 **2.2 Meteorological measurements**

203 Meteorological and radiation conditions were monitored at the Amundsen-Nobile Climate Change
204 Tower (Mazzola et al., 2016), located about 500 m west of the sampling site and from the AWIPEV
205 observatory (Maturilli et al., 2013), located about 800 m north of the sampling site. No
206 meteorological measurements are present in the sampling area. Temperature, relative humidity,
207 were measured at 2 m above ground level and were considered as representative of the atmosphere
208 just above the snow surface while wind speed and direction at 10 m above ground. Incoming solar
209 radiation was measured at the top of the CCT tower (33 m), this value was not influenced by
210 reflections from the structure. One-minute data were used to obtain hourly averages. Snow
211 accumulation data were obtained by measuring the high of 4 plastic poles located at the extremities
212 of the snow sampling field. Precipitation data were recorded in Ny-Ålesund by the Norwegian
213 Meteorological Institute (station n. 99910) and downloaded through the eKlima database
214 (eklima.no).

215

216 **2.3 Snow Mercury analysis**

217 Total Hg concentrations in surface snow samples was determined using a Thermo Element
218 Inductively Coupled Plasma Sector Field Mass Spectrometry (ICP-SFMS Element XR, Thermo-
219 Fisher, Bremen, Germany) in low resolution scanning mode using ^{202}Hg as the analytical mercury
220 mass with 10 replicates per sample measurement. The instrument was calibrated using standards
221 prepared from a mono-elemental Hg solution (TraceCert®, purity grade, Sigma-Aldrich, MO,
222 USA). Hg calibration standards were re-analysed every 10 samples as a quality control check. The
223 percent relative standard deviation (n=10) ranged from 0.5 % at 500 pgg^{-1} to 10 % at 1 pgg^{-1} and
224 amounted to 2.6 % on average. Considering the high volatility and instability of Hg in solution, the
225 samples were acidified at 2 % v/v with ultrapure hydrochloric acid before they were melted and
226 analyzed. Each sample was weighed and the exact amount of HCl was added to reach a final
227 concentration of 2 % (Planchon et al., 2004; Spolaor et al., 2018).

228

229 **2.4 Snow iodine, sodium and bromine analysis**

230 Halogens (I and Br) and sodium analyses were conducted on non-acidified samples. Total sodium
231 (Na), iodine (I) and bromine (Br) concentrations were determined by ICP-SFMS (Spolaor et al.,
232 2016c). Each analytical run started and ended with an ultra-pure water (UPW) cleaning session of 3
233 min to ensure a stable background level throughout the analysis. The external standards that were
234 used to calibrate the analytes were prepared by diluting a 1000 ppm stock IC (ion chromatography)
235 standard solution (TraceCERT® purity grade, Sigma-Aldrich, MO, USA). The standard
236 concentrations ranged between 10 and 4000 ng g^{-1} for sodium, 0.01 and 1 ngg^{-1} for iodine and
237 between 0.5 and 20 ng g^{-1} for bromine. The residual standard deviation (RSD) was low for all
238 analytes, the halogens ranged between 1–2% and 2–5% for Br and I, respectively, and the RSD was
239 3-4 % for sodium.

240

241 **2.5 Atmospheric mercury measurements**

242 **Atmospheric mercury concentrations were obtained from the Zeppelin Observatory located at 474**
243 **m a.s.l, less than 1 km away from the sampling site (Figure 1).** Gaseous elemental mercury (GEM)
244 was monitored using a Tekran 2537 Hg vapor analyzer as described by Aspmo et al., 2005 and as
245 summarized here: ambient air was sampled at 1.5 l min^{-1} through a Teflon filter via a heated
246 sampling line. A soda-lime trap was mounted in-line before the instrument filter. Hg in the air is
247 pre-concentrated for 5 minutes by amalgamation on two parallel gold cartridges, which alternate
248 between collection and thermal desorption, followed by AFS (atomic fluorescence spectrometric)
249 detection. The instrument was auto-calibrated every 25 hours using an internal Hg permeation
250 source, whose accuracy was verified during routine site audits that include manual injections of Hg
251 from an external source (Aspmo et al., 2005). **The measurements at Zeppelin were the only GEM**
252 **measurements available in the Ny-Alesund area. Although GEM measurements at the snow**

253 sampling site would have been more reliable in determining possible interactions between snow and
254 atmospheric mercury, it was not possible to set up an instrument at the site. We assume that the
255 snow reactions occurring at the sampling site at 40 m a.s.l. are of the same order of magnitude as
256 those occurring in the snow layers surrounding Zeppelin station.

257 3. Results

258 The 2015 and 2016 experiments were characterized by similar atmospheric conditions (except for
259 the incoming solar radiation) while during the 2017 experiment a storm approached Ny-Ålesund
260 during the first 12 hours of the experiment with strong winds lasting for the first 24 hours of the
261 experiment. During the 2015 experiment under full day conditions, the average air temperature
262 ranged between -10°C and -6°C and the surface snow temperature range between -13°C and -5°C ,
263 showing a diurnal variability connected with changes in the incoming solar radiation (Figure 2).
264 Incoming solar radiation ranged from a minimum of 25 Wm^{-2} to a maximum of 450 Wm^{-2} . Wind
265 speed was almost constant and remained below 3 ms^{-1} during most of the experiment, except for a
266 few hours at the beginning when it exceeded 3 ms^{-1} . Snowfall (1 cm net accumulation on the
267 ground) occurred on the 30th of April between 3 am and 11 am (Figure 2, pink rectangle). A snow
268 event, causing a net accumulation of 1 cm of snow, also occurred during the 2016 experiment
269 (Figure 3, pink rectangular) when day and night periods were present. The snow event occurred on
270 the 9th of April between 10 am and 3 pm. During the 2016 experiment, conducted between 6th and
271 the 9th of April, the snow temperature was not registered due a technical problem with the
272 temperature probe installed in the snow. Air temperature ranged between -7 and -3°C and solar
273 radiation between zero at night time to a maximum of 227 W/m^2 . As for the first experiment, wind
274 speed was below 3 ms^{-1} , minimizing the effect of blowing snow. Wind direction was almost
275 constant and prevailing from east. The GEM and the surface snow mercury datasets were de-
276 trended to emphasize the diurnal variation and remove the decreasing trend present in both datasets.
277 The de-trended series were obtained calculating the linear regression line for both series and
278 subtracting this value from the data. Figure 3 (middle panel) reports the de-trended mercury dataset
279 while the Figure 4 shows the raw data and the methods used to remove the trend. The 2017 winter
280 experiment (Figure 5) was characterized by a snowstorm that occurred on the 24th of January (10
281 hours after the experiment began, pink rectangle). Differently to the previous experiments, the wind
282 speed averaged 9 ms^{-1} during the storm, with a maximum speed of 16 ms^{-1} (Figure 5, orange line).
283 Strong winds can redistribute surface snow and significantly change chemical concentrations. For
284 these reasons, the winter experiment began on the 24th of January and ended on the 29th of January
285 for 5 days in total, compared the 3 days adopted for the 2015 and 2016 experiment. The length of
286 the experiment was extended of 2 days to minimize the impact of the strong wind and snowfall that
287 occurred at the beginning of the experiment. Air temperatures ranged from between -17°C and -3°C ,

288 while snow temperatures ranged between -25°C and -10°C (Figure 5, upper panel). One important
289 issue that could confound the results obtained by surface sampling is spatial variability. Spatial
290 variability was tested during the three experiments and specifically for the four elements
291 investigated. Six surface snow aliquots were collected at the beginning of each experiment within
292 the delimited area at the same time. The results obtained show that for sodium, bromine and
293 mercury, spatial variability can explain 10% of the variability whilst for iodine the variability was
294 of the order of 5%. Concentrations detected during the three experiments show different
295 background levels (Table 1) for total iodine, sodium, mercury and gaseous elemental mercury (Br
296 was measured only during the 2016 experiment). For sodium, the highest concentration was
297 detected during the 2015 (full day) experiment where concentrations in surface snow averaged 3500
298 ngg^{-1} . The lowest sodium concentrations were determined during the winter period with
299 concentrations of around 1500 ngg^{-1} . For iodine the trend was the opposite, with highest
300 concentrations in winter (0.38 ngg^{-1}) and the lowest during the 24h sunlight period (0.15 ngg^{-1}). For
301 total mercury, the minimum concentration was found in early spring (0.007 ngg^{-1} , 2016 experiment)
302 while the highest values were detected during 2015 (full light) and 2017 winter experiment (on
303 average 0.010 ngg^{-1} for 2015 and 0.009 ngg^{-1} for 2017). Gaseous elemental mercury **during the**
304 **experiments** had the highest concentration during springtime, when 24 h incoming solar radiation is
305 present (1.45 ngm^{-3}) while the lowest value has been detected during the polar night (1.28 ngm^{-3}).
306 The average concentration during the experiment is only representative for specific periods in the
307 experiment and should not be considered as a reference concentration for a specific season. **The**
308 **experimental periods were chosen to reduce the possibility of snowfall deposition during the**
309 **experiment and to avoid periods with strong wind and subsequent windblown snow transport (the**
310 **main reason why the winter experiment was lengthened to 5 days). This was all done to minimize**
311 **the effects of meteorological parameters on our results and make the experiments more comparable.**
312 **We cannot exclude that the behaviour that we found for iodine, mercury and bromine could be**
313 **significantly different during the specific season/periods (such as for example during an AMDE) or**
314 **when meteorological conditions such as snow deposition frequency and amount, wind strength and**
315 **cloud coverage were different.** Some indications emerged, especially for iodine, which showed the
316 highest concentrations during the polar night in the absence of solar radiation. Considering iodine
317 (inorganic and organic) is mainly emitted by oceanic processes, iodine concentrations were
318 normalized to sodium concentrations to obtain an iodine enrichment (I_{enr}) compared to the bulk
319 seawater abundance. This is defined as $I_{\text{enr}} = I_{\text{snow}} \times (\text{Na}_{\text{snow}} / [\text{Na}]_{\text{sw}})$, where $I/\text{Na} = 0.00000596$,
320 (Millero et al., 2008) where “sw” = measured sea water abundance. In the 2015 experiment (24h
321 sunlight), iodine had an average enrichment value of 5, a value that exponentially increased (up to
322 190) during snowfall (Figure 2), so if we consider the snowfall period the mean value increases to
323 10. The 2016 experiment (day/night) was characterized by a diurnal cycle for both mercury and

324 iodine (and I_{enr}) and by an average I_{enr} value of 11, with the lowest value during day time and higher
325 values detected during the night periods (Figure 3). As for the 2015 experiment, the experiment
326 conducted in 2016 was characterized by a snowfall event that significantly influenced the surface
327 iodine concentration and its enrichment factor. During the 2016 experiment, snowfall caused the I_{enr}
328 to increase up to 300. The rapid increase in iodine and its enrichment factor during snowfall was
329 followed by a rapid decrease to the pre-snowfall (seasonal background value) concentration during
330 the 2015 experiment (Figure 2), whilst in the 2016 experiment the increased concentration and
331 enrichment caused by the snow fall was most likely masked by the night time deposition (Figure 3).
332 Similar behaviour was measured for total mercury in surface snow samples, with an increase in
333 concentration during snowfall followed by a rapid decrease in both experiments (Figure 2 and 3).
334 The winter experiment is characterized by the highest iodine enrichment values (47 on average) and,
335 similar the previous experimental results, the experiment was characterized by snowfall and strong
336 winds during the first 24h. During the storm period in the winter experiment we detected an
337 increase in iodine concentrations (and I_{enr} up to 100), however the difference in iodine enrichment
338 between the snowfall periods and rest of samples collect was not statistically significant. The
339 average elemental concentrations for each experiment are reported in Table 1.

340

341 **4. Discussion**

342 The behaviour of mercury and iodine in surface snow depends on the season and the amount of
343 incoming solar radiation (Figure 2, Figure 3, Figure 5). **Atmospheric mercury depletion events**
344 **(AMDE) can occur during the springtime causing large-scale deposition of mercury to the snow**
345 **pack concurrently with ozone photochemistry and oxidation reactions involving bromine. During**
346 **our spring experiments we have not observed any rapid decreases in GEM or increases in mercury**
347 **concentrations in the surface snow. This indicates that no AMDE occurred during the sampling**
348 **periods and that, especially for bromine, the main depositional source was from sea spray given the**
349 **distance from the coast line (< 1km) and the positive correlation with Na (Table 2). This is inline**
350 **with the findings of (Angot et al., 2016a), who reported that AMDEs occur much less frequently at**
351 **Zeppelin station than they do at Alert or Station North in Greenland.**

352 During wintertime (Figure 5), iodine behaves similarly to sodium. Sodium does not undergo
353 photochemical processes in the snow and is often used to evaluate/correct for marine sea spray
354 emission/deposition (Spolaor et al., 2014). During winter, iodine has higher concentrations and
355 enrichment factors (compared to its sea water abundance based on the I/Na mass ratio). These
356 higher values in surface snow could be due to the absence of photochemical activation by solar
357 radiation. In the absence of photochemistry and with limited biological production in winter
358 (Ardyna et al., 2013), we expect to find enrichment values close to the seawater abundance.

359 However, during the 2017 experiment, iodine had higher than expected enrichment values
360 suggesting that an extra source(s), in addition to sea spray emission may exist and that it might be
361 dominant during winter. Saiz-Lopez et al. 2016 suggests that nighttime radical activation can occur.
362 They indicate that the reaction of HOI with NO_3 , to yield $\text{IO} + \text{HNO}_3$, is possible under winter
363 tropospheric conditions (Saiz-Lopez et al., 2016). The inclusion of this reaction, along with that of
364 $\text{I}_2 + \text{NO}_3$, has a number of significant implications, such as the night time activation of iodine
365 radical chemistry that can cause an enhanced night time oceanic emissions of HOI and I_2 (Saiz-
366 Lopez et al., 2016). **Although typical NO_x levels are low in the Arctic, the reaction with NO_3 could**
367 **be relevant close to Arctic cities and under episodes of anthropogenic long range transport of**
368 **pollution to the Arctic.** Sea spray aerosol droplets could absorb gas phase iodine emissions from the
369 ocean surface (as suggested by the high correlation between total iodine and sodium, Figure 5 and
370 Table 2) and deposited on the surface snow causing the high iodine surface snow enrichment. This
371 process, together with the absence of photoactivation that causes iodine loss from the snow surface,
372 could explain the high level of iodine during the polar night.

373 In parallel to iodine, our experiments have focused on the rapid changes in mercury concentrations
374 that could occur in surface snow during the polar night. This is because without these temporal
375 resolution measurements, it is extremely difficult to determine which reactions might be occurring.
376 During the first 24 hours of the winter experiment (2017) we had strong winds remodelling the
377 snow surface. Variations in surface mercury concentrations detected within the first 24 hours may
378 in part have been due to snowfall and physical artefacts caused by windblown snow redistribution.
379 After the storm, total mercury concentrations in surface snow tended to stabilize until the end of the
380 experiment. It should be noted that some oscillations in surface snow mercury concentrations and
381 the ambient air above have been detected. Mercury in the snow rapidly decreased from 00:00 on the
382 24th until noon on the same day and was associated with an increase in the atmospheric mercury
383 concentration (Figure 5). After this sharp increase, the GEM concentration decreased rapidly while
384 the surface snow mercury increased. These two rapid events occurred within about 24 hours,
385 supporting the idea of a connection and interchange between GEM and the mercury present in snow
386 surface, even during the night-time. Night-time mercury reactions have been thought to occur.
387 Angot et. al. 2016b suggested that mercury deposition onto the snow surface in the dark could be
388 due to several mechanisms, including gas-phase oxidation, heterogeneous reactions, or dry
389 deposition of $\text{Hg}(0)$ (Angot et al., 2016b; Song et al., 2018). This hypothesis however is based on
390 results obtained at Dome C on the Antarctic Plateau over the entire winter season, conditions very
391 different to those in Svalbard. The average mercury surface snow concentrations detected during
392 the winter experiment are comparable to those during the 2015 experiment (Figure 2 and Table 1),
393 this might be due, as for iodine, to the lack of light induced snow re-emission, but might also be
394 caused by different background concentrations independent of any seasonal effect.

395 The most interesting experiment is the one conducted during early April in 2016 when a day and
396 night cycle was still present (Figure 3). During this experiment, mercury and iodine, show a similar
397 pattern with a distinct diurnal cycle in surface snow (I_{snow} vs Hg_{snow} $R = 0.57$ $p\text{-value} < 0.01$). For
398 both elements, the highest concentrations were detected during the night and the lowest during the
399 day. Iodine has been demonstrated to be active in the upper snow layer. Previous laboratory and
400 outdoor experiments have demonstrated two photo-induced mechanisms for the release of inorganic
401 iodine from the snowpack to the atmosphere: i) photooxidation of iodide in ice with the resulting
402 production of tri-iodide (I_3^-) and evaporable molecular iodine (I_2) (Kim et al., 2016), and ii) the
403 emission of an iodine photofragments following the heterogenous photoreduction of iodate in ice
404 (Gálvez et al., 2016). These experimental studies have shown that the release of iodine from the
405 snow/ice to the atmosphere depends on solar radiation. Indeed, (Raso et al., 2017) recently
406 measured I_2 in the Arctic atmosphere under natural sunlight conditions with results that are in
407 agreement with the supposed photochemical production mechanisms.

408 Kim et al., 2016, showed that the iodide photooxidation to I_3^- strongly depended on irradiation time
409 following the UV-Visible absorption spectrum of iodide in ice. This would explain the observations
410 of reduced iodine concentrations in ice during the sunlit parts of the day. Although we do not have
411 observations of atmospheric iodine, it is very likely that snow re-emission during the day leads to a
412 peak in reactive gas phase iodine in the overlying polar boundary layer at low solar zenith angles.
413 The emitted gas phase iodine would then readily form reservoir species (HOI, $IONO_2$, HI) (Saiz-
414 Lopez et al., 2014) that once photochemistry ceases could deposit and accumulate in the snow/ice
415 until the following sunrise, when re-emission starts again.

416 Active mercury recycling from the snow pack has already been suggested/observed by several
417 authors (Dommergue et al., 2012; Durnford and Dastoor, 2011; Song et al., 2018; Steffen et al.,
418 2008). Mercury in its oxidized forms can be deposited onto the snowpack, increasing total Hg
419 concentrations in the upper snow strata. Once present in the snowpack, Hg is very labile, it can be
420 reduced back to $Hg(0)$ and can undergo dynamic exchange with the atmosphere above (Steffen et
421 al., 2002). **Atmospheric mercury can undergo wet or dry deposition to the snow pack, either as
422 gaseous elemental (GEM) or oxidised mercury (GOM), and can be reemitted as GEM (Brooks et al.
423 2006).** Photochemical reactions are important in altering the speciation of Hg in the snowpack and
424 depend on environmental properties and snowpack chemistry. Spolaor et al. 2018 shows that total
425 Hg concentrations in the surface snow in the inner Antarctic Plateau do not exhibit a clear diurnal
426 cycle as has been determined for gaseous elemental mercury (Angot et al., 2016c; Dommergue et
427 al., 2012). However Hg in surface snow shows the highest values during the insolation minima,
428 suggesting that its concentration in the snow might be influenced by daily differences in incoming
429 solar radiation. The experiment at Dome C (Spolaor et al. 2018) was carried out under full polar day
430 conditions with incoming solar radiation reaching the snow surface for the entire period of the

431 experiment. The experiment conducted at Ny-Ålesund between the 6th to the 9th of April 2016 was
432 characterized by a night and day cycle. Similar to iodine, a clear diurnal cycle has been detected for
433 atmospheric and surface snow mercury. Snow mercury shows the highest concentrations during the
434 night, with a minimum during the daytime (night periods are highlighted in Figure 3 by the grey
435 rectangular). Contrary to this, the GEM shows a minimum during the night-time and a maximum
436 during the daytime. This anti-phase behaviour (Figure 3 and Table 2) suggests that under day light
437 conditions, mercury in the surface snow can be reduced and released by photochemical processes
438 from the snow surface, resulting in increases in atmospheric concentrations. **This is not the only
439 mechanism that can lead to increases in atmospheric concentrations. Changes in the atmospheric
440 mixing layer height may lead to apparent concentration changes of atmospheric species, even if
441 total amounts in the boundary layer remain constant. In the Ny-Ålesund area it is difficult to
442 estimate the height of the boundary layer due to effects induced by winds and by the orography of
443 the Brøgger Peninsula. However, during the experiments the stable meteorological conditions
444 suggested that the atmospheric mixing height was quite stable, minimizing any influence of the
445 boundary layer on GEM concentrations.**

446 During the night, mercury can be oxidized to Hg(II) and re-deposited onto the snow surface. In
447 addition to this diurnal oscillation during the experiment, if we exclude the snowfall that caused a
448 re-enrichment of surface snow for both elements, we detected a decreasing trend for mercury in
449 snow as well as in the atmosphere (Figure 4 and Table 2), from the beginning to the end of the
450 experiment. This decreasing trend may be ascribed to re-emission during the daytime and an
451 incomplete deposition during the night due to possible dilution/removal processes caused by the
452 surrounding atmosphere, with air mass movements as well for mixing within the upper atmospheric
453 strata. This suggested atmospheric removal could explain the positive correlation between GEM
454 and snow surface Hg seen in Table 2 that is masking the antiphase caused by the diurnal daylight
455 cycle. When the two series are de-trended by removing the overall decreasing trend, (by
456 considering 6-hour average values) the correlation between atmospheric and snow mercury
457 becomes significantly negative (Figure 4 upper panel and Table 2).

458 At the end of the 2016 experiment, a snowfall event occurred (Figure 3 pink rectangular). The net
459 effect of the snowfall was to increase the mercury concentration in the upper snow surface.
460 Precipitation events seem to be associated with elevated total Hg concentrations in surface snow
461 samples (Figure 2 and Figure 3). Angot et al., 2016c have suggested that the presence of ice crystals
462 could enhance the dry deposition of Hg(II). Indeed, due to an elevated specific surface area, the
463 mercury-capture efficiency of ice crystals is high (Douglas et al., 2008). Although there is a
464 deposition of mercury to surface snow, atmospheric mercury did not show a decrease in
465 concomitance with the snowfall but continued to show the usual diurnal pattern. In Antarctica, it
466 has been demonstrated that snow and atmospheric mercury concentrations are related but it should

467 be taken into consideration that the boundary layer can be confined to the first 30 meters above the
468 snow surface (Angot et al., 2016a). After the snow fall the mercury surface snow concentration
469 decreased from 45 to 8 pgg^{-1} with a net loss of 37 pgg^{-1} of total mercury in 1 hour. Assuming all
470 snow mercury lost is lost as GEM, considering a sampling depth of 3 cm for an area of 1 m^2 and
471 considering an average snow density of 0.3 g cm^{-3} , the emission rate would be 5.5 $\text{ng m}^{-2} \text{h}^{-1}$, a
472 similar order of magnitude to that determined by Kamp et al. 2017. It must be noted that Kamp et al.
473 2017 measured the total emission flux while we focussed on the upper snow pack layer, emissions
474 from the lower/deeper strata are not considered that might contribute to the total emission from the
475 snow pack. The mercury released from the snow after snowfall may not be enough to impact the
476 GEM due to dilution effects. Is also possible that the Zeppelin station is located often above the
477 marine boundary layer and the mercury released from the snow is confined and is not able to
478 influence the mercury concentration in the free troposphere. Zeppelin station is at a higher elevation
479 (approximately 400 meters above the sampling site) compared to the snow-sampling site, but is the
480 only site giving hourly mercury atmospheric measurements in the area. Although the two sites may
481 not be directly connected (Aspmo et al., 2005), we assume that the snow mercury and iodine release
482 mechanisms that occur in the snow at our sampling site are also occurring in the snow surrounding
483 the Zeppelin station at more or less the same rates. Consequently, GEM atmospheric concentrations
484 and the diurnal cycle should be representative of the variations in the atmospheric cycle above the
485 surrounding sampled snow field.

486 Surface snow iodine concentrations, similarly to mercury, are enhanced during liquid or solid
487 deposition. Several studies have demonstrated that rain, snow and aerosol are enriched in soluble
488 organic iodine as well as inorganic iodine (iodide and iodate) (Baker, 2005; Saiz-Lopez and von
489 Glasow, 2012). Uptake of iodine species by cloud droplets and snowflakes followed by wet
490 deposition or snowfall are major atmospheric iodine removal processes, which would enhance the
491 concentration of iodine in the snow/ice. It is interesting to note that after the snowfall events, the
492 enhanced concentrations in surface snow rapidly decrease. This phenomenon is more evident during
493 the 2015 experiment (Figure 2) when 24 hours of solar irradiation occur. In the 2016 experiment
494 after the snowfall, the iodine decrease is probably masked by nocturnal deposition. Bromine was
495 also measured during the 2016 experiment (Figure 6) to understand if, as for iodine and mercury, it
496 can undergo surface recycling re-emission processes as suggest by previous studies (Simpson et al.,
497 2007). Bromine shows a correlation of $r = 0.85$ with sodium and, the Br_{enr} factor (calculated as
498 $\text{Br}_{\text{enr}} = \text{Br}_{\text{snow}} \times (\text{Na}_{\text{snow}} * [\text{Br}/\text{Na}]_{\text{sw}}$, where $\text{Br}/\text{Na}_{\text{sw}} = 0.006$), does not show a diurnal cycle as for
499 iodine (and its enrichment factor) and mercury. As has already been proposed, bromine after
500 deposition is probably preserved in surface snow (Spolaor et al. 2014). During snowfall, both
501 sodium and bromine decrease, most likely due to the dilution effect caused by new snowfall. It is
502 likely that the main sodium and bromine deposition occurred by sea spray deposition caused by

503 wave breaking (no sea ice was present in the fjord in front of Ny-Alesund during the experiments so
504 the bromine explosion over sea ice did not occur). Windblown snow and, eventual snowfall, can
505 affect the deposition of what is present in the atmosphere and dilute the concentrations in surface
506 snow. However, it should be noted that although Br and Na surface snow concentrations decrease
507 during snowfall, the Br enrichment factor increased, suggesting that snowfall is able to scavenge
508 gas phase bromine present in the atmosphere in addition to the aerosol phase and deposit it onto the
509 snow surface.

510 The experiment conducted in 2015 was characterized by full light conditions (Figure 2) similar to
511 those encountered in Antarctica (Spolaor et al., 2018). Both iodine and mercury in surface snow did
512 not show any diurnal cycle suggesting that a continuous recycling process may act on the snow
513 surface. Iodine shows an almost constant concentration in the first part of the experiment with some
514 oscillations, connected to sodium variations, hence possible sea spray deposition, occurring in the
515 second part of the experiment. While GEM still shows a clear diurnal cycle, the mercury in the
516 snow does not (Figure 2). The Hg concentration in the surface snow has some variations that are not
517 connected with changes in incoming solar radiation. As for the 2016 experiment, during the last
518 days of the experiment, a snowfall occurred, causing a rapid enrichment of iodine and Hg in the
519 surface snow followed by a rapid decrease most likely due to photo induced re-emission processes.

520

521 **5. Conclusions**

522 Three high temporal resolution experiments have been carried out between 2015 and 2017. The
523 three experiments were aimed at studying the behaviour of iodine and mercury (and bromine only
524 in 2016) in snow during the different polar seasons. One was conducted during the polar night (25th
525 to 29th of January 2017), one during the spring when the night and day cycle was present (6th to 10th
526 of April 2016) and one during late spring when sunlight was present for 24 hours a day (28th of
527 April to 1st of May 2015). The results obtained show that these elements have markedly different
528 behaviours in surface snow that are mainly governed by sunlight and snow deposition. For iodine,
529 the highest snow concentrations were detected during the winter polar night experiment (2017),
530 while the lowest were during late spring (2015) when continuous solar radiation reaches the snow
531 surface. For mercury the highest concentrations were detected in the winter (2017) and during late
532 spring experiment (2015).

533 Our high temporal resolution experiments did not have the aim of characterizing the average
534 surface snow concentrations but were designed to understand the behaviour of these elements in
535 surface snow within specific seasonal changes that can occur. A clear diurnal cycle for mercury and
536 iodine has been determined when a day and night cycle was still present, however, for Br (and its
537 enrichment factor) no diurnal cycle has been detected showing it has a more conservative behaviour
538 in snow. Total mercury concentrations in surface snow peak during the night and decreases during

539 the day, the opposite of its behaviour in the atmosphere. **The daily variation in atmospheric GEM**
540 **concentration might also be influence by changes in the boundary layer height, however the stable**
541 **meteorological conditions during the experiment tended to minimize this effect.** Iodine, acts
542 similarly to mercury, peaking during the night and decreasing during the day. Considering our
543 finding that up to 70% of the iodine present in the snow can be released to the atmosphere by photo-
544 induced reactions. the active role of snow in providing gas phase iodine should be considered in
545 studies of nucleation processes in the polar atmosphere.

546 This unique set of experiments has demonstrated for the first time the different behaviours of these
547 target elements under different irradiation conditions and demonstrate that snow is an active
548 substrate. The results obtained in Arctic snow could be translated to alpine regions and, more
549 generally, anywhere in the presence of snow. The diurnal cycle determined for mercury in the
550 Arctic, if demonstrated occurring in other places with high snow cover, could have an impact on
551 water resources, with higher concentrations of mercury deposited in the water basin at night. These
552 experiments have underlined some specific processes that can occur in surface snow, however
553 additional studies are planned to better understand the real impact of these processes on the
554 overlying atmosphere. **We hope that these results contribute to the efforts in understanding the role**
555 **of the snow pack in the Arctic mercury and iodine cycles and bromine behaviour in surface snow.**
556 **Understanding the behaviour of these elements in the surface snow-pack may shed light on the role**
557 **and the contribution of snow emissions, primarily to the marine boundary layer. For example,**
558 **species such as iodine, are directly active in the formation of cloud condensation nuclei that could**
559 **have a direct effect on polar climate.**

560
561

562 **Author contribution**

563 A.S., E.B., D.C. conceived the experiment; A.S., E.B., D.C., F.G., F.D. collected the samples; A.S.,
564 C.T., F.L., E.B. measured the samples; M.M., M.Mat. provide the meteorological and radiation data;
565 K.A.P. provide the mercury atmospheric data; A.S. ASL, WRLC, HA wrote the paper with inputs
566 from A.D., C.B., M.B.

567

568 **Acknowledgements**

569 This project has received funding from the European Union's Horizon 2020 research and innovation
570 programme under grant agreement No 689443 via project iCUPE (Integrative and Comprehensive
571 Understanding on Polar Environments). We thank the support received at the Dirigibile Italia Arctic
572 Station from the National Research Council — Department of Earth System Science and
573 Environmental Technologies (CNR-DSSTTA). We acknowledge the help of ELGA LabWater in
574 providing the PURELAB Pulse and PURELAB Flex which produced the ultrapure water used in
575 these experiments.

576 **TABLES**

577 **Table 1.** Concentration of iodine and its enrichment in surface snow (I_{snow} , I_{enr}), surface snow
 578 mercury (Hg_{snow}), atmospheric mercury (Hg_{atm}) and surface snow sodium (Na_{snow}) during the
 579 different experiments. Concentrations and standard deviation (in brackets) are calculated for the
 580 entire dataset; when marked with (*) indicates that the concentration has been calculated without
 581 considering the snow fall events.

582

	I_{snow} (ngg ⁻¹)	Na_{snow} (ngg ⁻¹)	Hg_{snow} (ngg ⁻¹)	Hg_{atm} (ngm ⁻³)	I_{enr}
2015 (day)	0.147 (0.162)	3442 (1180)	0.010 (0.006)	1.45(0.18)	10.7 (25.5)
2015*	0.090 (0.027)	3502 (1030)	0.009 (0.004)	1.46(0.19)	4.59 (1.43)
2016 (day\night)	0.167 (0.076)	2041 (777)	0.007 (0.008)	1.35 (0.13)	25.7 (46.4)
2016*	0.142 (0.057)	2317 (498)	0.007 (0.009)	1.40 (0.08)	10.2 (3.28)
2017 (night)	0.382 (0.175)	1518 (749)	0.009 (0.006)	1.26 (0.07)	44.3 (11.2)
2017*	0.433 (0.185)	1786 (770)	0.008 (0.004)	1.26 (0.06)	41.8 (8.40)

583

584

585 **Table 2.** Correlation coefficient between Iodine and sodium, bromine and sodium (only 2016) and
 586 atmospheric and snow mercury. The correlation is calculated for the entire dataset. When the
 587 correlation is marked with “*”, this indicates that the correlation has been calculated without
 588 considering the snow fall events. During the 2016 experiment the correlation between Hg_{snow} vs
 589 Hg_{atm} * has been detrended to highlight the antiphase between Hg_{atm} and Hg_{snow} . The plus and minus
 590 indicate if the association is positive or negative, which the values in parenthesis are the p-values.

591

	I vs Na	I vs Na^*	Br vs Na	Br vs Na^*	Hg_{snow} vs Hg_{atm}	Hg_{snow} vs Hg_{atm}^*
2015	0.24 (0.052)+	0.63 (<0.01)+	NA	NA	0.18 (0.13)+	0.36 (0.011)+
2016	0.21 (0.041)+	0.62 (<0.01)+	0.91 (<0.01)+	0.74 (<0.01)+	0.12 (<0.01)+	0.43 (<0.01)+**
2017	0.90 (<0.01)+	0.89 (<0.01)+	NA	NA	0.22 (0.05)+	0.062 (0.63)+

**detrended 0.61 (0.056)-

592

593

594

595

596

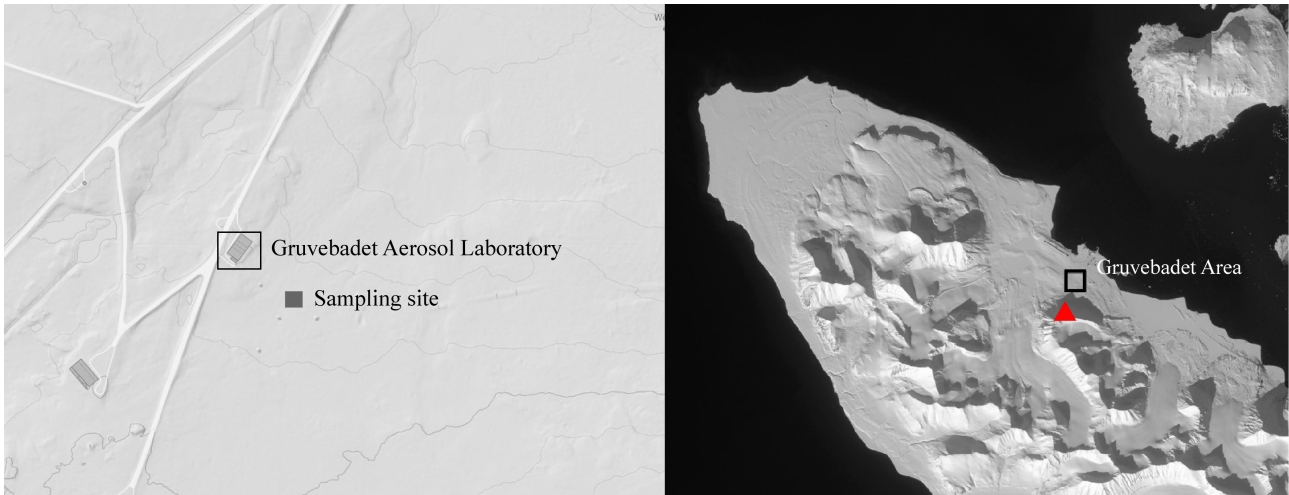
597

598

599 **FIGURES**

600

601 **Figure 1.** Location of the experimental area in the proximity of Ny-Ålesund research village (black
602 rectangular – right panel) and the site of experiments (grey rectangular – left panel) behind the
603 “Gruvebadet” Aerosol Laboratory. Red triangle shows the GEM measurements site. Maps from
604 toposvalbard.npolar.no.
605



606

607

608

609

610

611

612

613

614

615

616

617

618

619

620

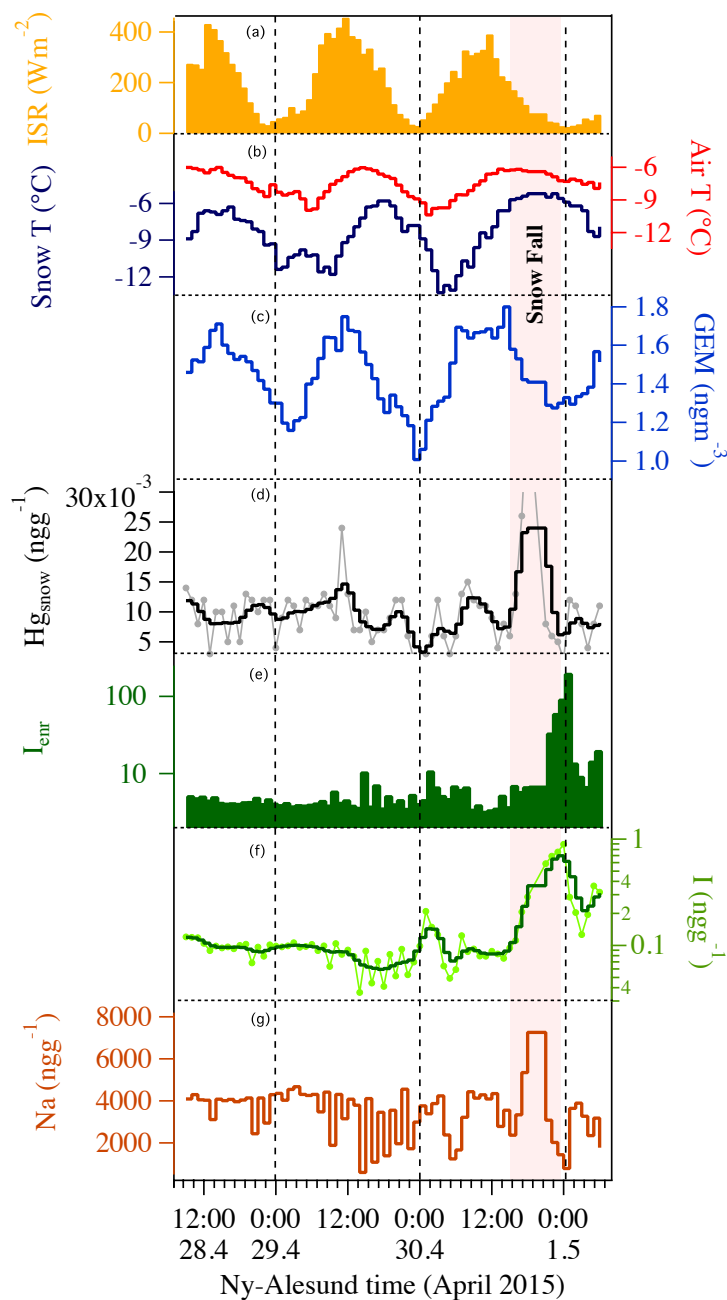
621

622

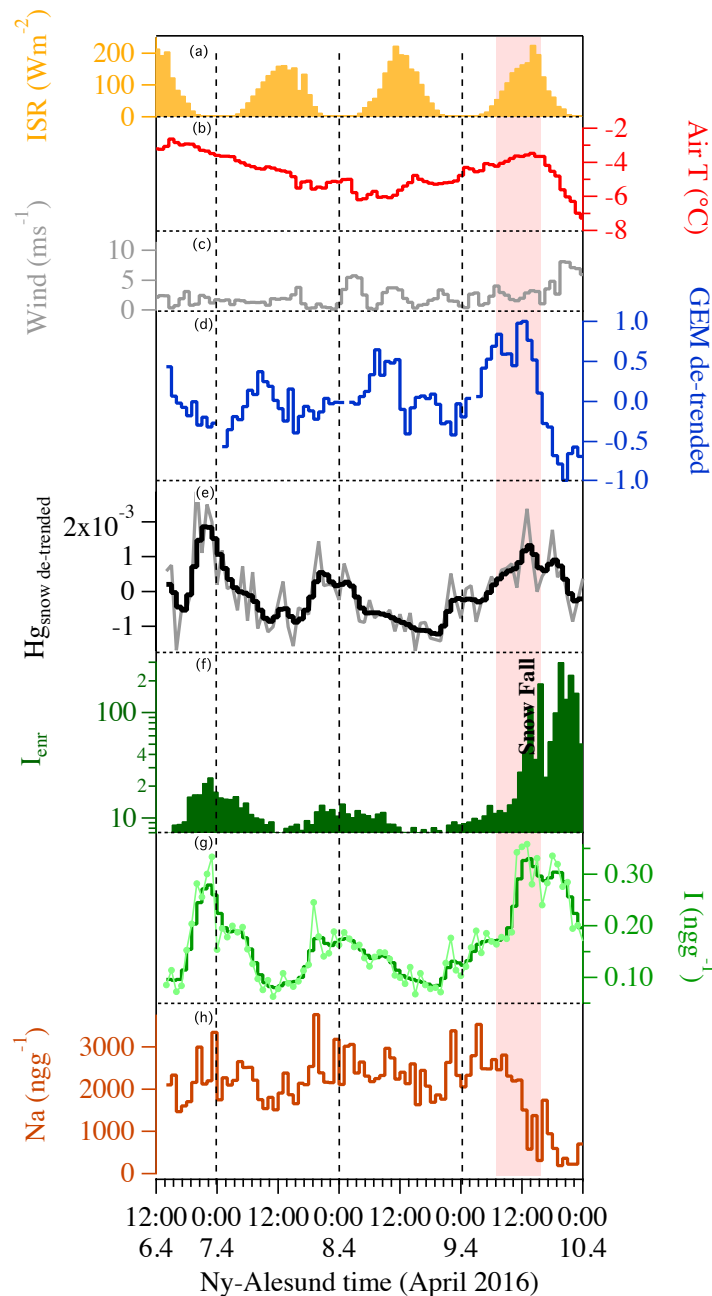
623

624

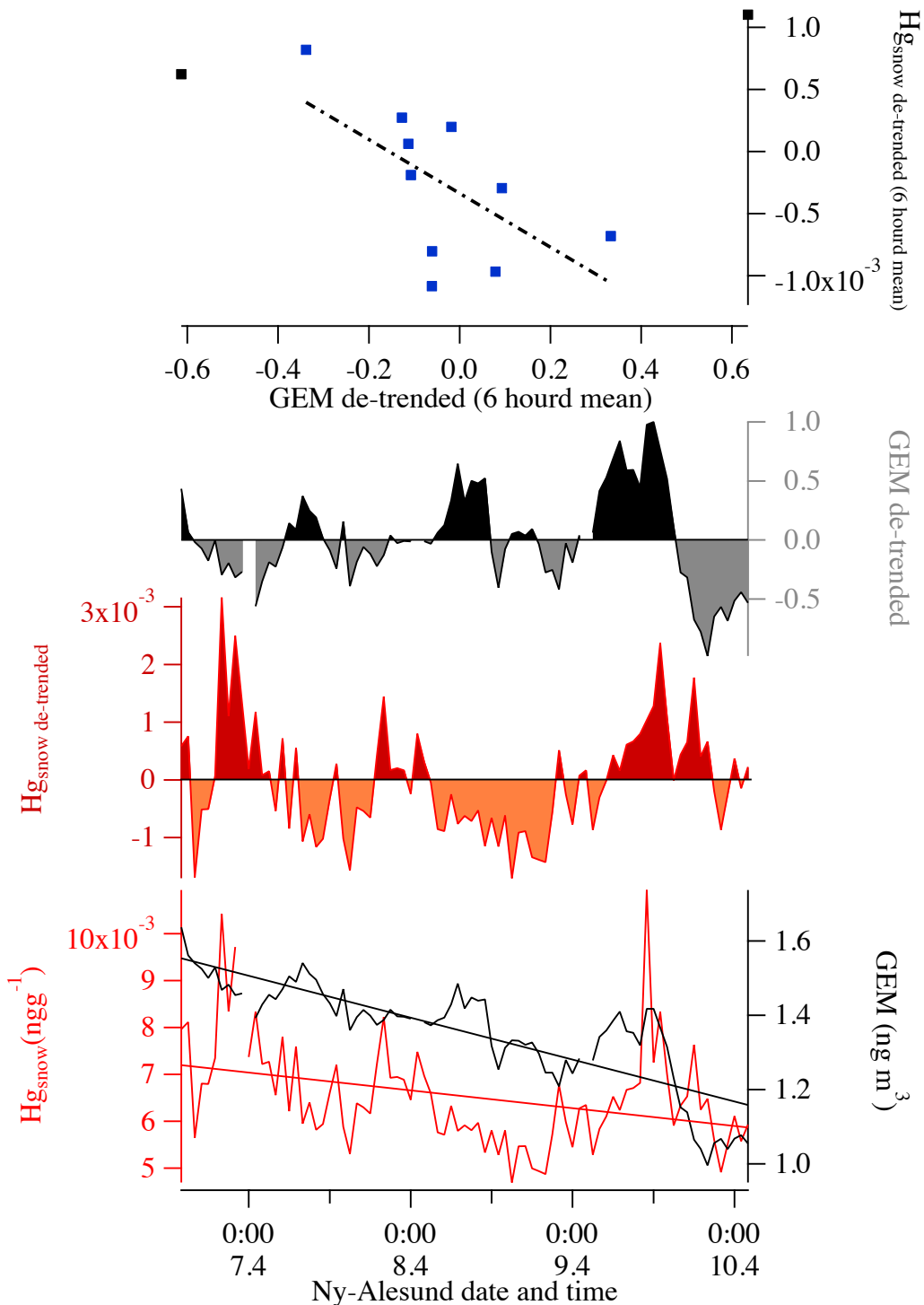
625 **Figure 2.** The 2015 experiment: continuous light conditions. The hourly sodium (g - dark red)
 626 concentrations are connected with iodine concentrations (f - light green for the raw data and green
 627 for the three-point smoothing) except during the snowfall where the signals decouple. Iodine
 628 enrichment (e - dark green) demonstrates the effect of snowfall on iodine concentration in surface
 629 snow. Gaseous elemental mercury (c - blue) exhibit a diurnal pattern while total mercury in surface
 630 snow (grey line and black line three-point smoothing) does not. Snowfall occurrence is highlighted
 631 by the pink rectangle. Snow and air temperature (d - dark blue and red) show the diurnal cycle
 632 connected with incoming solar radiation (ISR) (a - solid yellow). Wind speed is not shown since it
 633 was almost constant during the entire experiment. Dashed vertical lines indicate local midnight
 634 time.



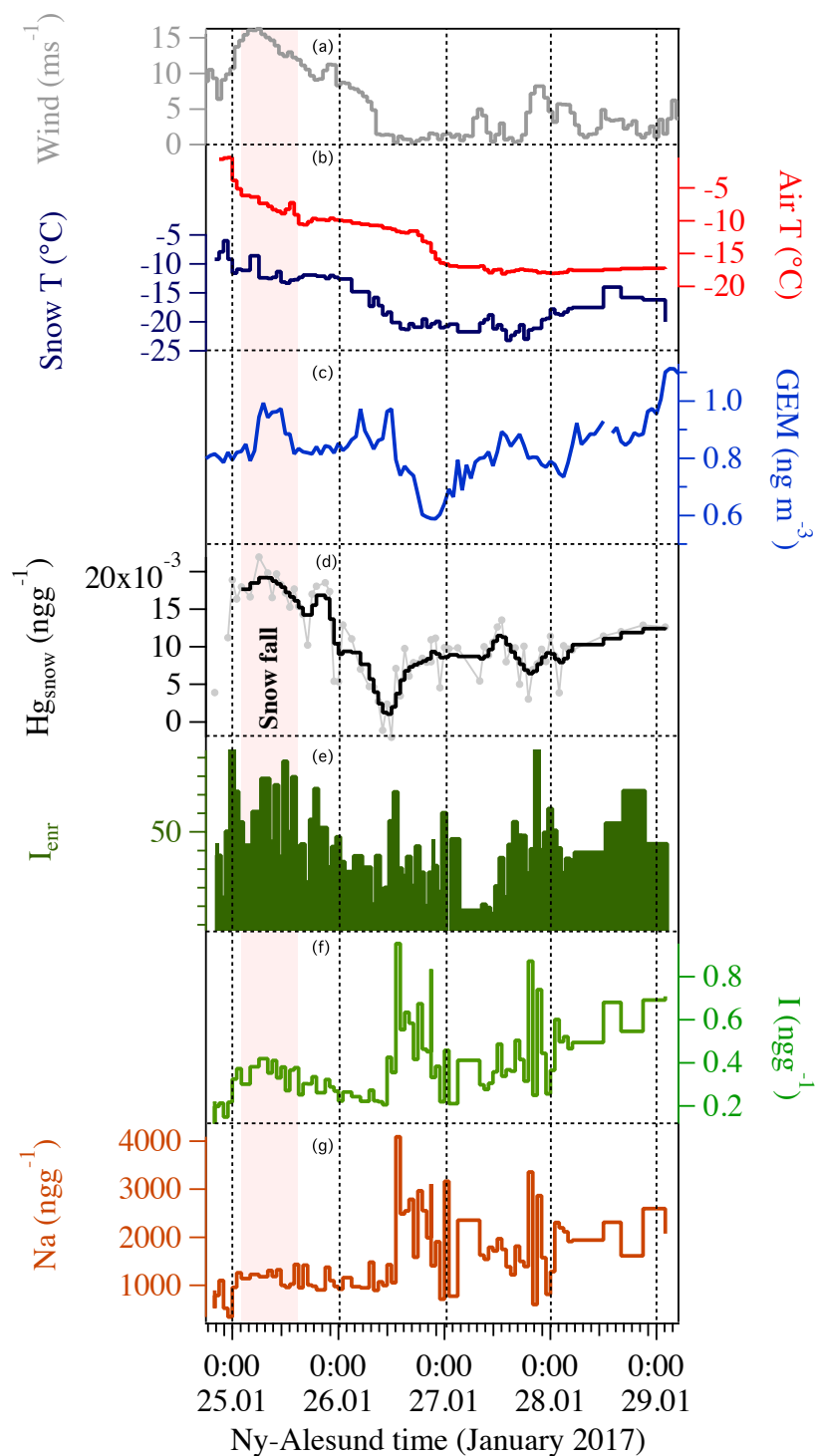
636 **Figure 3.** The 2016 experiment took place when a day and night cycle was available. Iodine
 637 concentration (g - light green line for the raw data and green light for the three-point smoothing)
 638 exhibited a diurnal variability (except during the snow fall event), not detected for sodium (h - dark
 639 red line). The Iodine enrichment factor (f - dark green solid line) also exhibited a diurnal cycle and
 640 highlights the effect of snowfall on iodine concentration in surface snow (pink rectangle shows the
 641 snow fall event). De-trended GEM (d - blue line) and the surface snow de-trended total mercury
 642 concentrations (grey lines for raw data and black line for the three-point smoothing) show opposing
 643 diurnal patterns. Additional information can be found in Figure 4. Air temperature does not show a
 644 pronounced diurnal cycle (b - red line) connected with incoming solar radiation (ISR)(a - yellow
 645 solid). Wind speed is shown in grey (c). Dashed vertical lines indicate local midnight time.



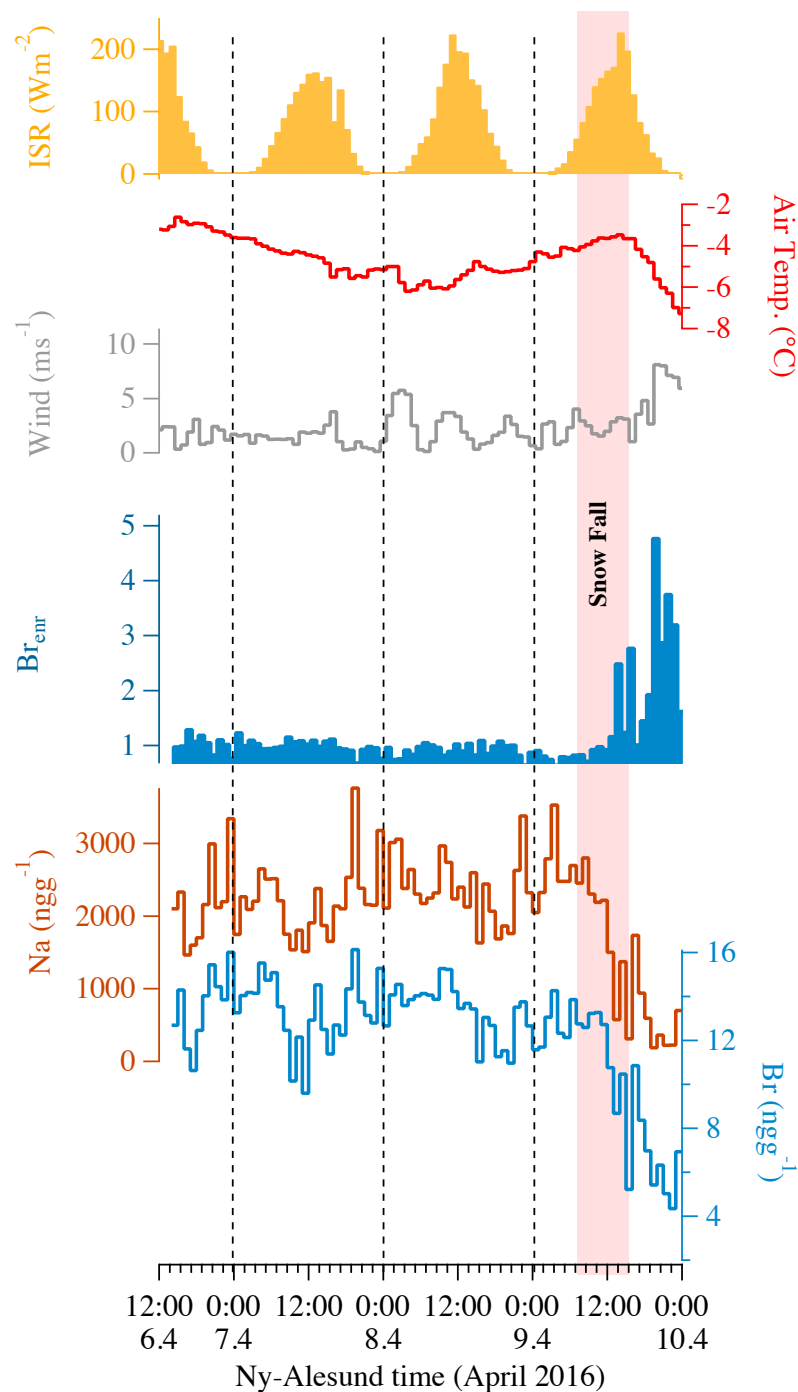
647 **Figure 4.** The lower panel shows the two series without any statistical treatment (Hg_{atm} =black;
 648 Hg_{snow} =red). The regression line obtained for surface snow mercury is $Hg_{snow}=-0.0004t + 16.136$,
 649 while for atmospheric mercury is $GEM=-0.1127t + 4787.8$. The middle panel shows the de-trended
 650 Hg series in surface snow (in red/orange) and atmosphere (grey/black). The upper panel shows the
 651 correlation between detrended Hg_{snow} and Hg_{atm} considering 6-hour average value. **The figure is**
 652 **based on the same data as Figure 3.**
 653



655 **Figure 5.** The 2017 experiment was conducted during the polar night. Iodine concentration (f -
 656 green line) correlated with sodium concentration (g - dark red line). The Iodine enrichment factor (e -
 657 dark green solid line) did not exhibit any diurnal cycle and had the higher value compare the three
 658 experiments. Gaseous elemental mercury (c - blue line) and the surface snow total mercury
 659 concentrations did not exhibit any diurnal pattern (d - light grey line for raw data and black line for
 660 three-point smoothed). Snow and air temperature (b - dark blue and red) did not show any diurnal
 661 cycle. Wind speed is shown in grey. Dashed vertical lines indicate local midnight time.



663 **Figure 6.** Surface Bromine recycle during the 2016 experiment. The Bromine concentration (light
 664 blue line) does not show a diurnal variability and follows the sodium surface concentration (dark
 665 red line). Bromine enrichment factor (blue solid line calculated as $Br_{enr} = Br_{snow} / (Na_{snow} \times 0.006)$
 666 where 0.006 is the Br\Na sea water mass ratio) do not show a diurnal cycle but it is evident that
 667 snowfall effects the bromine concentration and its enrichment factor during snowfall (pink
 668 rectangle). Air temperatures do not show a pronounced diurnal cycle (red line) connect with the
 669 incoming solar radiation (solid yellow). Dashed vertical lines indicate local midnight time.



670

671

- 673 Allan, J. D., Williams, P. I., Najera, J., Whitehead, J. D., Flynn, M. J., Taylor, J. W., Liu, D.,
674 Darbyshire, E., Carpenter, L. J., Chance, R., Andrews, S. J., Hackenberg, S. C., and McFiggans, G.:
675 Iodine observed in new particle formation events in the Arctic atmosphere during ACCACIA,
676 *Atmos. Chem. Phys.*, 15, 5599-5609, 2015.
- 677 Angot, H., Dastoor, A., De Simone, F., Gårdfeldt, K., Gencarelli, C. N., Hedgecock, I. M., Langer,
678 S., Magand, O., Mastromonaco, M. N., Nordstrøm, C., Pfaffhuber, K. A., Pirrone, N., Ryjkov, A.,
679 Selin, N. E., Skov, H., Song, S., Sprovieri, F., Steffen, A., Toyota, K., Travnikov, O., Yang, X., and
680 Dommergue, A.: Chemical cycling and deposition of atmospheric mercury in polar regions: review
681 of recent measurements and comparison with models, *Atmos. Chem. Phys.*, 16, 10735-10763,
682 2016a.
- 683 Angot, H., Dion, I., Vogel, N., Legrand, M., Magand, O., and Dommergue, A.: Multi-year record of
684 atmospheric mercury at Dumont d'Urville, East Antarctic coast: continental outflow and oceanic
685 influences, *Atmos. Chem. Phys.*, 16, 8265-8279, 2016b.
- 686 Angot, H., Magand, O., Helmig, D., Ricaud, P., Quennehen, B., Gallée, H., Del Guasta, M.,
687 Sprovieri, F., Pirrone, N., Savarino, J., and Dommergue, A.: New insights into the atmospheric
688 mercury cycling in central Antarctica and implications on a continental scale, *Atmos. Chem. Phys.*,
689 16, 8249-8264, 2016c.
- 690 Ardyna, M., Babin, M., Gosselin, M., Devred, E., Bélanger, S., Matsuoka, A., and Tremblay, J.-E.:
691 Parameterization of vertical chlorophyll a in the Arctic Ocean: impact of the subsurface chlorophyll
692 maximum on regional, seasonal, and annual primary production estimates, *Biogeosciences*, 10,
693 4383-4404, 2013.
- 694 Aspö, K., Gauchard, P.-A., Steffen, A., Temme, C., Berg, T., Bahlmann, E., Banic, C.,
695 Dommergue, A., Ebinghaus, R., Ferrari, C., Pirrone, N., Sprovieri, F., and Wibetoe, G.:
696 Measurements of atmospheric mercury species during an international study of mercury depletion
697 events at Ny-Ålesund, Svalbard, spring 2003. How reproducible are our present methods?,
698 *Atmospheric Environment*, 39, 7607-7619, 2005.
- 699 Baker, A. R.: Marine Aerosol Iodine Chemistry: The Importance of Soluble Organic Iodine,
700 *Environmental Chemistry*, 2, 295-298, 2005.
- 701 Björkman, M. P., Kühnel, R., Partridge, D. G., Roberts, T. J., Aas, W., Mazzola, M., Viola, A.,
702 Hodson, A., Ström, J., and Isaksson, E.: Nitrate dry deposition in Svalbard, *Tellus B; Vol 65 (2013)*,
703 2013. 2013.
- 704 Björkman, M. P., Vega, C. P., Kühnel, R., Spataro, F., Ianniello, A., Esposito, G., Kaiser, J., Marca,
705 A., Hodson, A., Isaksson, E., and Roberts, T. J.: Nitrate postdeposition processes in Svalbard
706 surface snow, *Journal of Geophysical Research: Atmospheres*, 119, 12,953-912,976, 2014.
- 707 Brage B. Hansen, Ketil Isaksen, Rasmus E. Benestad, Jack Kohler, Åshild Ø Pedersen, Leif E Loe,
708 Stephen J. Coulson, Jan Otto Larsen, and Varpe, Ø.: Warmer and wetter winters: characteristics
709 and implications of an extreme weather event in the High Arctic, *Environ. Res. Lett.*, 9, 2014.
- 710 Brooks, S., Arimoto, R., Lindberg, S., and Southworth, G.: Antarctic polar plateau snow surface
711 conversion of deposited oxidized mercury to gaseous elemental mercury with fractional long-term
712 burial, *Atmospheric Environment*, 42, 2877-2884, 2008.
- 713 Brooks, S. B., Saiz-Lopez, A., Skov, H., Lindberg, S. E., Plane, J. M. C., and Goodsite, M. E.: The
714 mass balance of mercury in the springtime arctic environment, *Geophys Res Lett*, 33, 2006.
- 715 Cuevas, C. A., Maffezzoli, N., Corella, J. P., Spolaor, A., Vallenga, P., Kjær, H. A., Simonsen,
716 M., Winstrup, M., Vinther, B., Horvat, C., Fernandez, R. P., Kinnison, D., Lamarque, J.-F.,
717 Barbante, C., and Saiz-Lopez, A.: Rapid increase in atmospheric iodine levels in the North Atlantic
718 since the mid-20th century, *Nature Communications*, 9, 1452, 2018.
- 719 Dall'Osto, M., Beddows, D. C. S., Tunved, P., Krejci, R., Ström, J., Hansson, H. C., Yoon, Y. J.,
720 Park, K.-T., Becagli, S., Udusti, R., Onasch, T., O'Dowd, C. D., Simó, R., and Harrison, R. M.:
721 Arctic sea ice melt leads to atmospheric new particle formation, *Scientific Reports*, 7, 3318, 2017.

722 Dommergue, A., Barret, M., Courteaud, J., Cristofanelli, P., Ferrari, C. P., and Gallée, H.: Dynamic
723 recycling of gaseous elemental mercury in the boundary layer of the Antarctic Plateau, *Atmos.*
724 *Chem. Phys.*, 12, 11027-11036, 2012.

725 Dommergue, A., Ferrari, C. P., Gauchard, P.-A., Boutron, C. F., Poissant, L., Pilote, M., Jitaru, P.,
726 and Adams, F. C.: The fate of mercury species in a sub-arctic snowpack during snowmelt,
727 *Geophysical Research Letters*, 30, n/a-n/a, 2003a.

728 Dommergue, A., Ferrari, C. P., Poissant, L., Gauchard, P.-A., and Boutron, C. F.: Diurnal Cycles of
729 Gaseous Mercury within the Snowpack at Kuujjuarapik/Whapmagoostui, Québec, Canada, *Environ*
730 *Sci Technol*, 37, 3289-3297, 2003b.

731 Dommergue, A., Sprovieri, F., Pirrone, N., Ebinghaus, R., Brooks, S., Courteaud, J., and Ferrari, C.
732 P.: Overview of mercury measurements in the Antarctic troposphere, *Atmos. Chem. Phys.*, 10,
733 3309-3319, 2010.

734 Douglas, T. A., Sturm, M., Simpson, W. R., Blum, J. D., Alvarez-Aviles, L., Keeler, G. J., Perovich,
735 D. K., Biswas, A., and Johnson, K.: Influence of Snow and Ice Crystal Formation and
736 Accumulation on Mercury Deposition to the Arctic, *Environ Sci Technol*, 42, 1542-1551, 2008.

737 Durnford, D. and Dastoor, A.: The behavior of mercury in the cryosphere: A review of what we
738 know from observations, *Journal of Geophysical Research: Atmospheres*, 116, n/a-n/a, 2011.

739 Faïn, X., Grangeon, S., Bahlmann, E., Fritsche, J., Obrist, D., Dommergue, A., Ferrari, C. P., Cairns,
740 W., Ebinghaus, R., Barbante, C., Cescon, P., and Boutron, C.: Diurnal production of gaseous
741 mercury in the alpine snowpack before snowmelt, *Journal of Geophysical Research: Atmospheres*,
742 112, 2007.

743 Ferrari, C. P., Gauchard, P.-A., Aspö, K., Dommergue, A., Magand, O., Bahlmann, E., Nagorski,
744 S., Temme, C., Ebinghaus, R., Steffen, A., Banic, C., Berg, T., Planchon, F., Barbante, C., Cescon,
745 P., and Boutron, C. F.: Snow-to-air exchanges of mercury in an Arctic seasonal snow pack in Ny-
746 Ålesund, Svalbard, *Atmos Environ*, 39, 7633-7645, 2005.

747 Førland, E. J., Benestad, R., Hanssen-Bauer, I., Haugen, J. E., and Skaugen, T. E.: Temperature and
748 Precipitation Development at Svalbard 1900-2100, *Advances in Meteorology*, 2011, 14, 2011.

749 Frieb, U., Deutschmann, T., Gilfedder, B. S., Weller, R., and Platt, U.: Iodine monoxide in the
750 Antarctic snowpack, *Atmos. Chem. Phys.*, 10, 2439-2456, 2010.

751 Gabrieli, J., Carturan, L., Gabrielli, P., Kehrwald, N., Turetta, C., Cozzi, G., Spolaor, A., Dinale, R.,
752 Staffler, H., Seppi, R., dalla Fontana, G., Thompson, L., and Barbante, C.: Impact of Po Valley
753 emissions on the highest glacier of the Eastern European Alps, *Atmos. Chem. Phys.*, 11, 8087-8102,
754 2011.

755 Gálvez, Ó., Baeza-Romero, M. T., Sanz, M., and Saiz-Lopez, A.: Photolysis of frozen iodate salts
756 as a source of active iodine in the polar environment, *Atmos. Chem. Phys.*, 16, 12703-12713, 2016.

757 Gilfedder, B. S., Petri, M., and Biester, H.: Iodine and bromine speciation in snow and the effect of
758 orographically induced precipitation, *Atmos Chem Phys*, 7, 2661-2669, 2007.

759 Han, Y., Huh, Y., Hong, S., Hur, S. D., and Motoyama, H.: Evidence of air-snow mercury exchange
760 recorded in the snowpack at Dome Fuji, Antarctica, *Geosciences Journal*, 18, 105-113, 2014.

761 Kamp, J., Skov, H., Jensen, B., and Sørensen, L. L.: Fluxes of gaseous elemental mercury (GEM) in
762 the High Arctic during atmospheric mercury depletion events (AMDEs), *Atmos. Chem. Phys.*, 18,
763 6923-6938, 2018.

764 Karner, F., Obleitner, F., Krismer, T., Kohler, J., and Greuell, W.: A decade of energy and mass
765 balance investigations on the glacier Kongsvegen, Svalbard, *Journal of Geophysical Research:*
766 *Atmospheres*, 118, 3986-4000, 2013.

767 Kim, K., Yabushita, A., Okumura, M., Saiz-Lopez, A., Cuevas, C. A., Blaszczyk-Boxe, C. S., Min,
768 D. W., Yoon, H.-I., and Choi, W.: Production of Molecular Iodine and Tri-iodide in the Frozen
769 Solution of Iodide: Implication for Polar Atmosphere, *Environ Sci Technol*, 50, 1280-1287, 2016.

770 Kohler, J. and Aanes, R.: Effect of Winter Snow and Ground-Icing on a Svalbard Reindeer
771 Population: Results of a Simple Snowpack Model, *Arctic, Antarctic, and Alpine Research*, 36, 333-
772 341, 2004.

773 Kohler, J., James, T. D., Murray, T., Nuth, C., Brandt, O., Barrand, N. E., Aas, H. F., and Luckman,
774 A.: Acceleration in thinning rate on western Svalbard glaciers, *Geophys Res Lett*, 34, 2007.

775 López-Moreno, J. I., Boike, J., Sanchez-Lorenzo, A., and Pomeroy, J. W.: Impact of climate
776 warming on snow processes in Ny-Ålesund, a polar maritime site at Svalbard, *Global and Planetary*
777 *Change*, 146, 10-21, 2016.

778 Lu, J. Y., Schroeder, W. H., Barrie, L. A., Steffen, A., Welch, H. E., Martin, K., Lockhart, L., Hunt,
779 R. V., Boila, G., and Richter, A.: Magnification of atmospheric mercury deposition to polar regions
780 in springtime: The link to tropospheric ozone depletion chemistry, *Geophys Res Lett*, 28, 3219-
781 3222, 2001.

782 Maturilli, M., Herber, A., and König-Langlo, G.: Climatology and time series of surface
783 meteorology in Ny-Ålesund, Svalbard, *Earth Syst. Sci. Data*, 5, 155-163, 2013.

784 Mazzola, M., Tampieri, F., Viola, A. P., Lanconelli, C., and Choi, T.: Stable boundary layer vertical
785 scales in the Arctic: observations and analyses at Ny-Ålesund, Svalbard, *Q J Roy Meteor Soc*, 142,
786 1250-1258, 2016.

787 Millero, F. J., Feistel, R., Wright, D. G., and McDougall, T. J.: The composition of Standard
788 Seawater and the definition of the Reference-Composition Salinity Scale, *Deep Sea Research Part I:*
789 *Oceanographic Research Papers*, 55, 50-72, 2008.

790 Moore, C. W., Obrist, D., Steffen, A., Staebler, R. M., Douglas, T. A., Richter, A., and Nghiem, S.
791 V.: Convective forcing of mercury and ozone in the Arctic boundary layer induced by leads in sea
792 ice, *Nature*, 506, 81-84, 2014.

793 Moroni, B., Becagli, S., Bolzacchini, E., Busetto, M., Cappelletti, D., Crocchianti, S., Ferrero, L.,
794 Frosini, D., Lanconelli, C., Lupi, A., Maturilli, M., Mazzola, M., Perrone, M. G., Sangiorgi, G.,
795 Traversi, R., Udisti, R., Viola, A., and Vitale, V.: Vertical Profiles and Chemical Properties of
796 Aerosol Particles upon Ny-Ålesund (Svalbard Islands), *Advances in Meteorology*, 2015, 11,
797 2015.

798 Moroni, B., Cappelletti, D., Crocchianti, S., Becagli, S., Caiazzo, L., Traversi, R., Udisti, R.,
799 Mazzola, M., Markowicz, K., Ritter, C., and Zielinski, T.: Morphochemical characteristics and
800 mixing state of long range transported wildfire particles at Ny-Ålesund (Svalbard Islands), *Atmos*
801 *Environ*, 156, 135-145, 2017.

802 Obrist, D., Agnan, Y., Jiskra, M., Olson, C. L., Colegrove, D. P., Hueber, J., Moore, C. W., Sonke,
803 J. E., and Helmig, D.: Tundra uptake of atmospheric elemental mercury drives Arctic mercury
804 pollution, *Nature*, 547, 201, 2017.

805 Planchon, F. A. M., Gabrielli, P., Gauchard, P. A., Dommergue, A., Barbante, C., Cairns, W. R. L.,
806 Cozzi, G., Nagorski, S. A., Ferrari, C. P., Boutron, C. F., Capodaglio, G., Cescon, P., Varga, A.,
807 and Wolff, E. W.: Direct determination of mercury at the sub-picogram per gram level in polar
808 snow and ice by ICP-SFMS, *J Anal Atom Spectrom*, 19, 823-830, 2004.

809 Poulain, A. J., Amyot, M., Findlay, D., Telor, S., Barkay, T., and Hintelmann, H.: Biological and
810 photochemical production of dissolved gaseous mercury in a boreal lake, *Limnology and*
811 *Oceanography*, 49, 2265-2275, 2004.

812 Raso, A. R. W., Custard, K. D., May, N. W., Tanner, D., Newburn, M. K., Walker, L., Moore, R. J.,
813 Huey, L. G., Alexander, L., Shepson, P. B., and Pratt, K. A.: Active molecular iodine
814 photochemistry in the Arctic, *Proceedings of the National Academy of Sciences*, 114, 10053, 2017.

815 Saiz-Lopez, A., Fernandez, R. P., Ordóñez, C., Kinnison, D. E., Gómez Martín, J. C., Lamarque, J.
816 F., and Tilmes, S.: Iodine chemistry in the troposphere and its effect on ozone, *Atmos. Chem. Phys.*,
817 14, 13119-13143, 2014.

818 Saiz-Lopez, A., Mahajan, A. S., Salmon, R. A., Bauguitte, S. J. B., Jones, A. E., Roscoe, H. K., and
819 Plane, J. M. C.: Boundary Layer Halogens in Coastal Antarctica, *Science*, 317, 348-351, 2007.

820 Saiz-Lopez, A., Plane, J. M. C., Baker, A. R., Carpenter, L. J., von Glasow, R., Gomez Martin, J. C.,
821 McFiggans, G., and Saunders, R. W.: Atmospheric Chemistry of Iodine, *Chem. Rev.*, 112, 1773-
822 1804, 2012.

823 Saiz-Lopez, A., Plane, J. M. C., Cuevas, C. A., Mahajan, A. S., Lamarque, J. F., and Kinnison, D.
824 E.: Nighttime atmospheric chemistry of iodine, *Atmos. Chem. Phys.*, 16, 15593-15604, 2016.

825 Saiz-Lopez, A., Plane, J. M. C., McFiggans, G., Williams, P. I., Ball, S. M., Bitter, M., Jones, R. L.,
826 Hongwei, C., and Hoffmann, T.: Modelling molecular iodine emissions in a coastal marine

827 environment: the link to new particle formation, *Atmospheric Chemistry and Physics*, 6, 883-895,
828 2006.

829 Saiz-Lopez, A., Sitkiewicz, S. P., Roca-Sanjuán, D., Oliva-Enrich, J. M., Dávalos, J. Z., Notario, R.,
830 Jiskra, M., Xu, Y., Wang, F., Thackray, C. P., Sunderland, E. M., Jacob, D. J., Travnikov, O.,
831 Cuevas, C. A., Acuña, A. U., Rivero, D., Plane, J. M. C., Kinnison, D. E., and Sonke, J. E.:
832 Photoreduction of gaseous oxidized mercury changes global atmospheric mercury speciation,
833 transport and deposition, *Nature Communications*, 9, 4796, 2018.

834 Saiz-Lopez, A. and von Glasow, R.: Reactive halogen chemistry in the troposphere, *Chemical*
835 *Society Reviews*, 41, 6448-6472, 2012.

836 Schroeder, W. H. and Munthe, J.: Atmospheric mercury—An overview, *Atmos Environ*, 32, 809-
837 822, 1998.

838 Sherman, L. S., Blum, J. D., Johnson, K. P., Keeler, G. J., Barres, J. A., and Douglas, T. A.: Mass-
839 independent fractionation of mercury isotopes in Arctic snow driven by sunlight, *Nature Geosci*, 3,
840 173-177, 2010.

841 Simpson, W. R., von Glasow, R., Riedel, K., Anderson, P., Ariya, P., Bottenheim, J., Burrows, J.,
842 Carpenter, L. J., Friess, U., Goodsite, M. E., Heard, D., Hutterli, M., Jacobi, H. W., Kaleschke, L.,
843 Neff, B., Plane, J., Platt, U., Richter, A., Roscoe, H., Sander, R., Shepson, P., Sodeau, J., Steffen, A.,
844 Wagner, T., and Wolff, E.: Halogens and their role in polar boundary-layer ozone depletion, *Atmos*
845 *Chem Phys*, 7, 4375-4418, 2007.

846 Sipilä, M., Sarnela, N., Jokinen, T., Henschel, H., Junninen, H., Kontkanen, J., Richters, S.,
847 Kangasluoma, J., Franchin, A., Peräkylä, O., Rissanen, M. P., Ehn, M., Vehkamäki, H., Kurten, T.,
848 Berndt, T., Petäjä, T., Worsnop, D., Ceburnis, D., Kerminen, V.-M., Kulmala, M., and O'Dowd, C.:
849 Molecular-scale evidence of aerosol particle formation via sequential addition of HIO₃, *Nature*, 537,
850 532, 2016.

851 Skov, H., Brooks, S. B., Goodsite, M. E., Lindberg, S. E., Meyers, T. P., Landis, M. S., Larsen, M.
852 R. B., Jensen, B., McConville, G., and Christensen, J.: Fluxes of reactive gaseous mercury
853 measured with a newly developed method using relaxed eddy accumulation, *Atmos Environ*, 40,
854 5452-5463, 2006.

855 Song, S., Angot, H., Selin, N. E., Gallée, H., Sprovieri, F., Pirrone, N., Helmig, D., Savarino, J.,
856 Magand, O., and Dommergue, A.: Understanding mercury oxidation and air–snow exchange on the
857 East Antarctic Plateau: a modeling study, *Atmos. Chem. Phys.*, 18, 15825-15840, 2018.

858 Spolaor, A., Angot, H., Roman, M., Dommergue, A., Scarchilli, C., Vardè, M., Del Guasta, M.,
859 Pedeli, X., Varin, C., Sprovieri, F., Magand, O., Legrand, M., Barbante, C., and Cairns, W. R. L.:
860 Feedback mechanisms between snow and atmospheric mercury: Results and observations from field
861 campaigns on the Antarctic plateau, *Chemosphere*, 197, 306-317, 2018.

862 Spolaor, A., Barbaro, E., Christille, J. M., Kirchgeorg, T., Giardi, F., Cappelletti, D., Turetta, C.,
863 Bernagozzi, A., Björkman, M. P., Bertolini, E., and Barbante, C.: Evolution of the Svalbard annual
864 snow layer during the melting phase, *Rendiconti Lincei*, doi: 10.1007/s12210-015-0500-8, 2016a.
865 1-8, 2016a.

866 Spolaor, A., Gabrieli, J., Martma, T., Kohler, J., Björkman, M. B., Isaksson, E., Varin, C.,
867 Vallelonga, P., Plane, J. M. C., and Barbante, C.: Sea ice dynamics influence halogen deposition to
868 Svalbard, *The Cryosphere*, 7, 1645-1658, 2013a.

869 Spolaor, A., Opel, T., McConnell, J. R., Maselli, O. J., Spreen, G., Varin, C., Kirchgeorg, T.,
870 Fritzsche, D., Saiz-Lopez, A., and Vallelonga, P.: Halogen-based reconstruction of Russian Arctic
871 sea ice area from the Akademii Nauk ice core (Severnaya Zemlya), *The Cryosphere*, 10, 245-256,
872 2016b.

873 Spolaor, A., Vallelonga, P., Gabrieli, J., Martma, T., Björkman, M. P., Isaksson, E., Cozzi, G.,
874 Turetta, C., Kjær, H. A., Curran, M. A. J., Moy, A. D., Schönhardt, A., Blechschmidt, A. M.,
875 Burrows, J. P., Plane, J. M. C., and Barbante, C.: Seasonality of halogen deposition in polar snow
876 and ice, *Atmos. Chem. Phys.*, 14, 9613-9622, 2014.

877 Spolaor, A., Vallelonga, P., Plane, J. M. C., Kehrwald, N., Gabrieli, J., Varin, C., Turetta, C., Cozzi,
878 G., Kumar, R., Boutron, C., and Barbante, C.: Halogen species record Antarctic sea ice extent over
879 glacial-interglacial periods, *Atmos. Chem. Phys.*, 13, 6623-6635, 2013b.

880 Spolaor, A., Vallelonga, P., Turetta, C., Maffezzoli, N., Cozzi, G., Gabrieli, J., Barbante, C., Goto-
881 Azuma, K., Saiz-Lopez, A., Cuevas, C. A., and Dahl-Jensen, D.: Canadian Arctic sea ice
882 reconstructed from bromine in the Greenland NEEM ice core, *Scientific Reports*, 6, 33925, 2016c.
883 Steffen, A., Douglas, T., Amyot, M., Ariya, P., Aspmo, K., Berg, T., Bottenheim, J., Brooks, S.,
884 Cobbett, F., Dastoor, A., Dommergue, A., Ebinghaus, R., Ferrari, C., Gardfeldt, K., Goodsite, M. E.,
885 Lean, D., Poulain, A. J., Scherz, C., Skov, H., Sommar, J., and Temme, C.: A synthesis of
886 atmospheric mercury depletion event chemistry in the atmosphere and snow, *Atmos. Chem. Phys.*,
887 8, 1445-1482, 2008.
888 Steffen, A., Schroeder, W., Bottenheim, J., Narayan, J., and Fuentes, J. D.: Atmospheric mercury
889 concentrations: measurements and profiles near snow and ice surfaces in the Canadian Arctic
890 during Alert 2000, *Atmospheric Environment*, 36, 2653-2661, 2002.
891 Udisti, R., Bazzano, A., Becagli, S., Bolzacchini, E., Caiazzo, L., Cappelletti, D., Ferrero, L.,
892 Frosini, D., Giardi, F., Grotti, M., Lupi, A., Malandrino, M., Mazzola, M., Moroni, B., Severi, M.,
893 Traversi, R., Viola, A., and Vitale, V.: Sulfate source apportionment in the Ny-Ålesund (Svalbard
894 Islands) Arctic aerosol, *Rendiconti Lincei*, 27, 85-94, 2016.
895 Vecchiato, M., Barbaro, E., Spolaor, A., Burgay, F., Barbante, C., Piazza, R., and Gambaro, A.:
896 Fragrances and PAHs in snow and seawater of Ny-Ålesund (Svalbard): Local and long-range
897 contamination, *Environmental Pollution*, 242, 1740-1747, 2018.
898 Wang, J., Zhang, L., and Xie, Z.: Total gaseous mercury along a transect from coastal to central
899 Antarctic: Spatial and diurnal variations, *Journal of Hazardous Materials*, 317, 362-372, 2016.
900 Westermann, S., Boike, J., Langer, M., Schuler, T. V., and Etzelmüller, B.: Modeling the impact of
901 wintertime rain events on the thermal regime of permafrost, *The Cryosphere*, 5, 945-959, 2011.
902 Zangrando, R., Barbaro, E., Zennaro, P., Rossi, S., Kehrwald, N. M., Gabrieli, J., Barbante, C., and
903 Gambaro, A.: Molecular Markers of Biomass Burning in Arctic Aerosols, *Environ Sci Technol*, 47,
904 8565-8574, 2013.
905
906